Scientific Inquiry and Review (SIR)
Volume 4, Issue 2, June 2020
ISSN (P): 2521-2427, ISSN (E): 2521-2435
Journal DOI: https://doi.org/10.32350/sir
Issue DOI: https://doi.org/10.32350/sir.42
Homepage: https://journals.umt.edu.pk/index.php/SIR/Home
Journal QR Code:

Article	**First-Principle Study of the Structural, Electronic, and Optical, Properties of Cubic Cesium Lead Halide Perovskites for Photovoltaic System**
Author(s)	Muhammad Waqas
Online Published	June 2020
Article DOI	https://doi.org/10.32350/sir.42.01
QR Code of Article	M. Waqas
To cite this Article	Waqas M. First-principle study of structural, electronic, and optical, properties of cubic cesium lead halide perovskites for photovoltaic system. *Sci Inquiry Rev.* 2020;4(2): 01–16. Crossref
Copyright Information	

Indexing & Abstracting

A publication of the
School of Science, University of Management and Technology
Lahore, Pakistan.

First-Principle Study of the Structural, Electronic, and Optical Properties of Cubic Cesium Lead Halide Perovskites for Photovoltaic System

Muhammad Waqas*

Department of Education

Government of the Punjab, Pakistan

*waqassarwari64@gmail.com

Abstract

Lead halide perovskites have attracted considerable attention as optoelectronic materials because these materials have high photovoltaic conversion efficiency [1]. The current study is based on Density Functional Theory (DFT). This theory was used to calculate the structural, optical, and electronic properties of the lead halide perovskites $CsPbX_3$ (X = Chlorine (Cl), Bromine (Br), Iodine (I)) compounds [2]. In order to calculate the above mentioned properties of cubic perovskites $CsPbX_3$ (X = Cl, Br, I), Full Potential Linear Augmented Plane Wave (FP-LAPW) method was implemented in conjunction with DFT utilizing LDA, GGA-PBE and mBJ approximations [3]. A good agreement was found between experimentally measured values and theoretically calculated lattice constants. These compounds have a direct and wide band gap located at the point of R-symmetry, while the band gap decreases from 'Cl' to 'I' down the group [4]. The densities of electrons revealed a strong ionic bond between Cs and halides and a strong covalent bond between 'Pb' and (Cl, Br, and I). The dielectric functions (reflectivity, refractive indices, absorption coefficients), optical conductivities (real and imaginary part) and other optical properties indicated that these compounds have novel energy harvester applications [5]. The modeling of these perovskite compounds shows that they have high absorption power and direct band gaps in visible ultraviolet range and it also shows that these compounds have potential applications in solar cells [6].

***Keywords*:** DFT, electronic properties, GGA, PBE, perovskites, solar cells

Introduction

Perovskites exhibit many engrossing properties from both theoretical and experimental point of views. In this particular analysis aimed to

simulate the bulk level higher symmetry, methyl ammonium cation (CH3NH3) was replaced with cesium (Cs) cation because the size of 'Cs' and its spherical symmetry are similar to that of CH3NH3 [7, 8]. It is a theoretical study of the electronic, optical and structural properties of metal halide cubic perovskites CsPbX3 (X=I, Cl, Br), carried out by applying Full Potential Linearized Augmented Plane Wave (FP-LAPW) method. In this approach, Local Density Approximation (LDA) is used for exchange-correlation. Such type of perovskites are frequently used in optoelectronics because they are suitable materials for high energy irradiations of optical devices [9].

1.1. Computational Details

To evaluate the structural, electronic and optical properties of cesium lead halide perovskites $MPbX_3$ (M = Cs and X = Cl, Br, I), the framework of DFT (using the solution of Kohn-Sham equations in FP-LAPW) was used [10]. The exchange-correlation potential was calculated using LDA, Generalized Gradient Approximation (GGA) and modified Becke-Johnson Exchange Potential (mBJ). For all atoms, input parameters, K points, RK_{max}, and G_{max} were preferred as 1000, 12 and 9. Furthermore, the muffin tin radius sphere was taken as 2.5 (bohr) [11]. Brillouin zone summation was performed using [2 x 2 x 2] grid points in the Brillouin zone. For splitting the valance from the core state, the energy threshold was selected to be -6.0 Ryd. Wyckoff positions for the atoms 'Cs', 'Pb' and 'I' were chosen as (0.5, 0.5, 0.5), (0, 0, 0) and (0.5, 0, 0), respectively with Pm3m-200 space group [12].

2. Results and Discussion

2.1. Structural Properties

The energy volume diagram obtained through the calculations of different volume energies using Murnaghan equation. It elaborates some important properties namely crystal lattice, equilibrium volume, bulk modulus and its derivatives [13]. The experimentally calculated lattice constant of $CsPbX_3$ (X = Cl, Br, I) was 6.29 A^o. These calculations (using LDA, GGA-PBE approximations) agree with other experimental and theoretical efforts (Figure 1) [14].

The calculated results for $CsPbX_3$ (X = Cl, Br, I), such as lattice constants, cohesive energy, energy bands and bulk modulus are shown in Table 1. For 'Cl', 'Br' and 'I', the calculated lattice constants for cubic structured $CsPbX_3$ (X = Cl, Br, I) were 5.7373 A^o, 5.998 A^o, and

6.38 A^o, respectively. These results agree with the experimental values, that is, 5.605A^o, 5.874 A^o and 6.33 A^o [15]. The calculated data given in Table 1 shows that the value of 'a' (A^o) increases by moving from Cl to I due to the increasing atomic size of anion. There are reasonable similarities between the calculated and theoretical values.

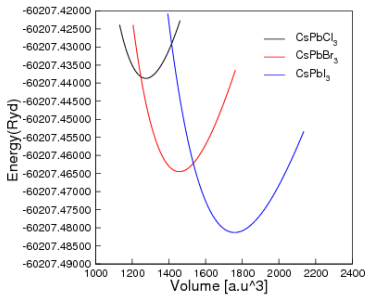

Figure 1. Variation of total energy as a function of unit cell volume

Table 1. Calculated Structural Parameters

Parameters	$CsPbCl_3$	$CsPbBr_3$	$CsPbI_3$
a_o(A^o)	5.7373	5.998	6.38
B (GPa)	21.80	18.54	14.70
B'	4.31	4.94	4.81
E_g(eV)	3.21	2.48	1.99
$\varepsilon_1(0)$	3.1	3.71	4.79

2.2. Band Structure Curves

The band structures of our compound were found to have direct band gaps. The band structure (energy function vs. k vectors) was plotted in the first Brillouin zone [16]. Important information about the crystal including the type of energy gap (direct or indirect), electronic nature of being metal or nonmetal and the mobility of carriers was obtained. One more direct band gap was observed at the M-point, above the minimum state of conduction band (Fig 1.2). Using mBJ approximation, the band structure of $CsPbX_3$ (X = Cl, Br, I) was calculated. The difference between the states at the maximum of valance band and the minimum of conduction band gave the value of electronic band gap [17]. The maximum and minimum states of valance band and conduction band were positioned at the R-point of the Brillouin zone [18]. The calculated band gaps (3.21 eV, 2.48 eV, and

1.99 eV) indicate a good agreement with experimental band gaps (3.0 eV, 2.3 eV and 1.73 eV). It can be noted that band gap decreased from 'Cl' to 'I' (Table 1) [19].

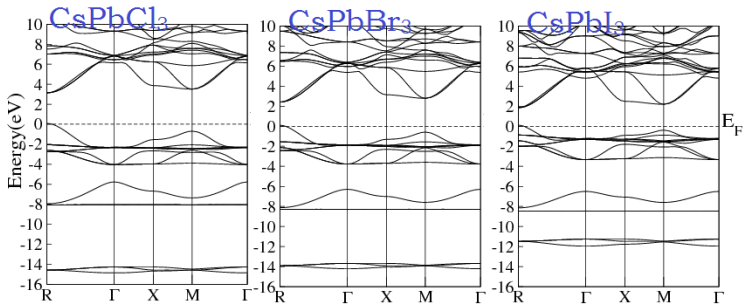

Figure 2. Energy band structures in a high symmetry direction

2.3. Density of States Curve

The probability of electrons' distribution in energy spectrum is described by Density of States (DOS). For the cubic phase of $CsPbX_3$ (X = Cl, Br, I), Total Density of States (TDOS) and Partial Density of States (PDOS) were calculated using GGA and mBJ approximations [20]. All features of TDOS remained the same. The values of TDOS of $CsPbX_3$ (X = Cl, Br, I) were 3.97eV, 3.70eV and 3.17eV, respectively. However, by replacing anions from 'Cl' to 'I' one by one, the valance and conduction bands were moved towards the Fermi level that was taken as zero reference point (Figure 3) [21].

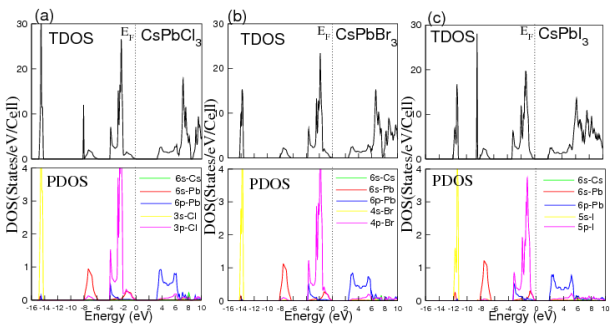

Figure 3. Total Density of States (TDOS) and Partial Density of States (PDOS)

It was observed that TDOS split into three different regions. Region I was of a lower valance band (around -14.9 to 14 eV) containing a fine band, which was due to the contribution of Cs-5p and Pb-6s states [22].

Region II was of upper valance band within the range (-4.0 to 0 eV), in which I-5p and Pb-6s states mostly contributed in the respective compound [23]. The lower part of the band was close to the Fermi level mostly due to the mixing of Pb-6p states with Cs-4d state, whereas its upper part was due to the Cs-4f state. Actually, the electronic level of 'Cs' was localized in the valance and conduction bands, so it did not contribute to the states nearest to the Fermi level [24].

2.4. Optical Properties Curve

The efficiency of photovoltaic devices for renewable energy production is generally determined by optical properties. These properties of the relevant materials are based on their various characteristics, for example, dielectric constant, electrical conductivity, reflection, absorption and power factor which are not constant for all materials [25].

The most fascinating function in solid state physics is the dielectric function which is also a complex function. This function contains real and imaginary part ($\varepsilon_1, \varepsilon_2$) of dielectric (Figure 4 (a, b)) [26].

The real part (ε_1) at equilibrium pressure started from zero energy and maximum peaks were recorded at 7.41, 5.39, 4.40, 2.58 eV, 3.34eV and 4.1 eV values of energy, respectively. The conduction was very weak at large values of ' ε_1 '. So, it showed that the real part and the conductivity of dielectric functions are reverse in relationship [27]. In the region between 15.20 eV to 17.35 eV, no wave propagated through the matter where dielectric function ' ε_1 ' was negative (Figure 4a).

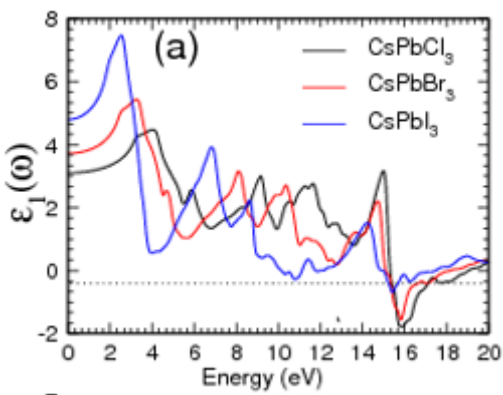

Figure 4a. Real part of dielectric constant

The entire optical parameters such as reflection, refraction and absorption were obtained from the real and imaginary parts of the dielectric function [28]. The imaginary part (ε_2) described the absorption behavior of $CsPbX_3$ (X = Cl, Br, I). It defined the disturbance produced by electromagnetic radiations. The absorption peaks were sharp and had greater magnitude for $CsPbI_3$ as compared to $CsPbBr_3$and $CsPbCl_3$, which was due to the narrower width of the valance band of $CsPbI_3$. It is clear from Figure 4a that the structures moved towards a lower energy from, that is, 'Cl' to 'I' (Figure 4b) [29].

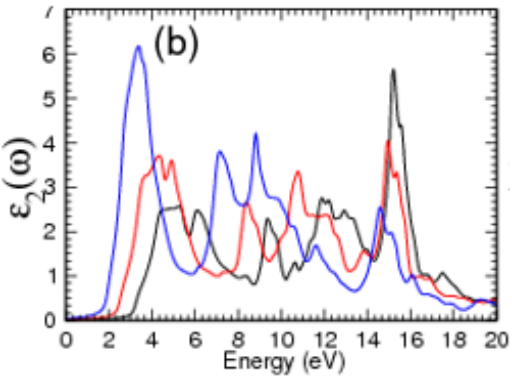

Figure 4b. Imaginary part of dielectric constant

For the appropriate use of an optical device, it is important to know about the refractive index of the material used. The variations in the refractive indices of the compound $CsPbX_3$ (Cl, Br, I) were displayed [30]. It was observed that the obtained curves at equilibrium pressure started from zero energy with 1.75, 1.92, and 2.20 values of refractive indices 'n'. The plotted graph shows that refractive indices decreased by increasing the radiated energy [31]. The peaks of the graph of the compound $CsPbX_3$ (Cl, Br, I) were observed as 2.65 eV, 3.42 eV, and 4.18 eV. It was found that cubic perovskites $CsPbX_3$ (Cl, Br, I) have maximum refractive indices between 1.75 and 2.5 to the light in the visible range 2.4-4.2 eV (Figure 4c) [32].

Electromagnetic waves had a low extinction coefficient when they passed through matter. The graphs of extinction coefficient of the compound $CsPbX_3$ (Cl, Br, I) show their maximum and minimum values at different values of energy [33]. We obtained the first maximum value of extinction coefficient, that is, 1.67 at 15.65 eV (Figure 4d). At that range of energy, we observed a major amount of

absorption of light which can also be confirmed from Fig. 5b. At the first minimum value of extinction coefficient, that is, 6 eV, the absorption of incident light was minimum [34].

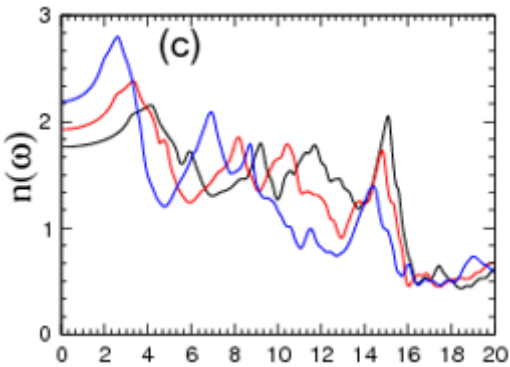

Figure 4c. Refractive index of $CsPbX_3$ (X = Cl, Br, I)

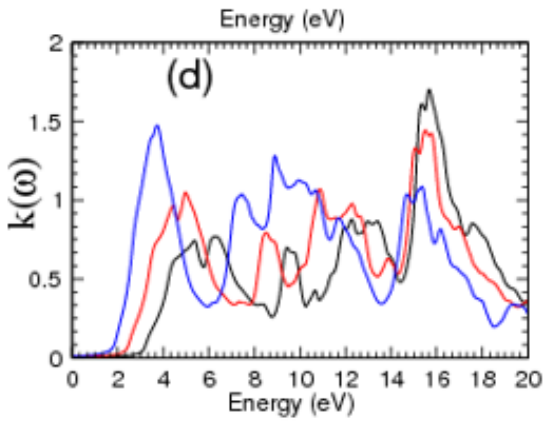

Figure 4d. Extension constant of $CsPbX_3$ (X = Cl, Br, I)

In the reflection coefficient graphs, reflectivity started from zero energy at 0.07, 0.1 and 0.14 [35]. The minimum reflection of light was lying at 5.45 eV, 13.67 eV and 18.97 eV. In comparison with Fig. 5a and Fig. 4c, there was a direct relation between refractive index and reflection of light. Moreover, reflectivity decreased while moving from 'Br' to 'I' and at the same time, refractive indices decreased while moving from 'I' to 'Br' (Figure 5a) [36].

The coefficient of absorption started from energy 2.0 eV 2.54 eV and 3.30 eV [37]. The highest peaks of graph were observed at 270, 225 and 167 at the energy values 15.70 eV, 15.54 eV and 15.37 eV,

respectively. It showed that absorption begins with the range of visible light and is increased by increasing the radiant energy of light. It was clear that absorption decreased while moving from 'Cl' to 'I' (Figure 5b) [38]. This was also the case with optical conductivity shown in figure 5c. The highest conductivity was of 'Cl' as compared to 'Br' and 'I'.

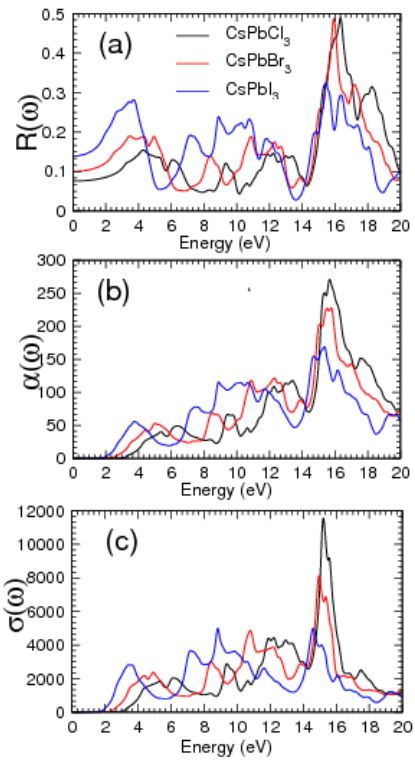

Figure 5. a) Reflective coefficient b) absorption coefficient c) optical coefficient

The quantification of the flow of free charge carriers is known as electrical conductivity. It is clear that the graphs began from a low temperature region (200 K). At room temperature (300K) electrical conductivity was 0.183 x $10^{19}(\Omega.\cdot m\cdot s)^{-1}$, 0.250 x $10^{19}(\Omega.\cdot m\cdot s)^{-1}$, and 0.187 x $10^{19}(\Omega.\cdot m\cdot s)^{-1}$ [39]. It was also showed that $CsPbBr_3$ was a good electrical conductor relative to $CsPbCl_3$ and $CsPbI_3$. The values of conductivity at 800K were 0.277 x $10^{19}(\Omega.\cdot m\cdot s)^{-1}$, 0.28 x 10^{19} $(\Omega.\cdot m\cdot s)^{-1}$, and 0.27 x $10^{19}(\Omega.\cdot m\cdot s)^{-1}$ (Fig. 6a).

To determine the efficiency of thermocouples Seebeck coefficient was used, that is, the ratio of potential difference and temperature difference. It was observed that the Seebeck coefficient of $CsPbX_3$ (X = Cl, Br, I) increased by increasing the temperature [40]. Seebeck coefficient at 300K was 103 $\mu V/k$ 87.2 $\mu V/k$, and 90.38.2 $\mu V/k$, whereas at 800K the values were 174 $\mu V/k$, 165 $\mu V/k$ and 173.84 $\mu V/k$, respectively (Fig. 6b) [41].

Due to the existence of electrons and lattice vibrations in the materials, heat conduction occurred. The main source of heat conduction in semiconductors is lattice vibration (Phonon) [42]. Thermal conductivity was increased as the temperature increased rapidly. It was clear that the value of thermal conductivity was 0.17 W/mKs at low temperature (300 k) and the thermal conductivity of this compound sharply increased. At 800 k, the thermal conductivity was maximum at 1.1 x 10^{14}W/mKs, 1.07 x 10^{14}W/mKs, 1.2 x 10^{14}W/mKs (Figure 6c) [43].

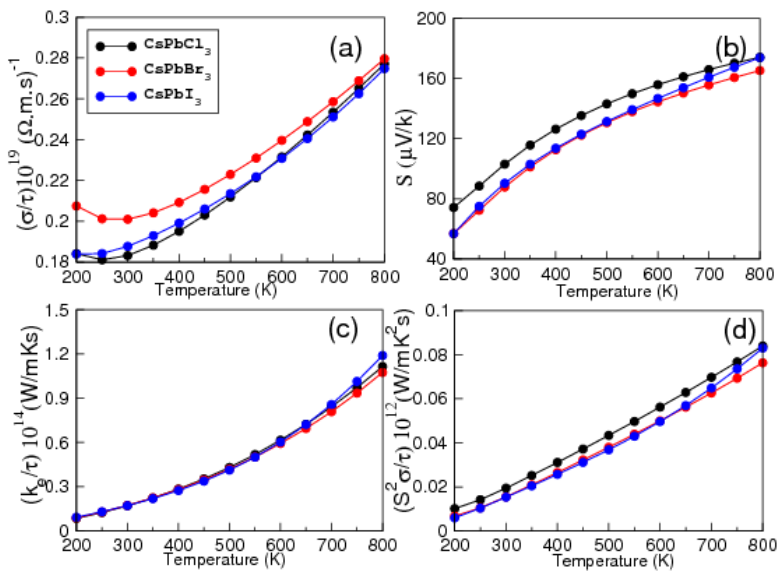

Figure 6. a) electrical conduction b) seeback coefficient c) thermal conduction d) power factor

The peaks of the power factor of $CsPbX_3$ (X = Cl, Br, I) at 300K were 0.02 W/mK^2, 0.015 W/mK^2 and 0.01 W/mK^2, respectively. At 800K, the values were 0.08 W/mK^2, 0.076 W/mK^2 and 0.08 W/mK^2,

respectively. It was observed that the power factor increased with temperature (Figure 6d) [44].

3. Conclusion

The key factors of structural, electronic and optical properties of the lead halide based inorganic cubic perovskites $CsPbX_3$ (X = Cl, Br, I) were studied in the current research using FP-LAPW method within the framework of LDA, GGA-PBE and mBJ approximations in equilibrium pressure that gave better energy gaps at the R-symmetry point nearest to the experimental results [45]. Computer modeling calculations showed a growth in lattice constants and unit cell energy (ground state), as well as the reduction in bulk modulus when halide ion changed from Cl to I. The ionic nature of Cs-halide has an inverse relation with the covalent nature of Pb-halide [46]. The calculated results also indicated that direct and wide band gaps exist in all compounds of $CsPbX_3$ (X = Cl, Br, I).

The calculated results indicated that due to the decrease in band gap from 'Cl' to 'I' the reflective and refractive indices increased, while optical conductivity and absorption coefficients decreased in value [47, 48]. It was found that in the visible and ultraviolet regions there were direct band gaps, direct transition and high absorption that generate a huge potential in these materials and they have potential applications for optoelectronic devices [49].

These decided results are close to the preliminary data. In spite of the fact that CsPbX3 (X = Cl, Br, I) gives best presentations, yet it has some characteristic issues on account of its lead content. In case Pb can be displaced from Sn or Bi, that issue can be constrained. Thus, this data can be used to develop a Pb free perovskite material for daylight based cell applications.

References

[1] Moreira RL, Dias A. Comment on prediction of lattice constant in cubic perovskites. *J Phys Chem Solids.* 2007; 68(8): 1617–1622.

[2] Trots DM, Myagkota SV. High-temperature structural evolution of caesium and rubidium triiodoplumbates. *J Phys Chem Solids.* 2008;69(10): 2520–2526.

[3] Nikl M, Nitsch K, Chval J. Optical and structural properties of ternary nanoaggregates in CsI-PbI2 co-evaporated thin films. *J*

Phys: Condens Matter. 2000;12(8): 1939. doi: 10.1088/0953-8984/12/8/335

[4] Verma AS, Kumar A, Bhardwaj SR. Correlation between ionic charge and the lattice constant of cubic perovskite solids. *Phys Status Solidi B*. 2008;245(8): 1520–1526.

[5] Dualeh A, mehi T, Tétreault N, et al. "Impedance spectroscopic analysis of lead iodide perovskite-sensitized solid-state solar cells. *ACS Nano*. 2013;8(1): 362–373.

[6] Burschka J, Pellet N, Moon S-J, et al. Sequential deposition as a route to high-performance perovskite-sensitized solar cells. *Nature*. 2013;499(7458): 316–319. doi: 10.1038/nature12340

[7] Zheng, J, Deng X, Zhou X, et al. Efficient formamidinium–methylammonium lead halide perovskite solar cells using Mg and Er co-modified TiO 2 nanorods. *J Mater Sci: Mater Electron*. 2019;30(12): 11043–11053.

[8] Yun JS, Seidel J, Kim J, et al. Critical role of grain boundaries for ion migration in formamidinium and methylammonium lead halide perovskite solar cells. *Adv Energy Mater*. 2016;6(13): 1600330.

[9] Ahmad M, Rehman G, Ali L, et al. Structural, electronic and optical properties of CsPbX3 (X= Cl, Br, I) for energy storage and hybrid solar cell applications. *J Alloys Compd*. 2017;705: 828–839.

[10] Begum R, Chin XY, Damodaran B, et al. Cesium lead halide perovskite nanocrystals prepared by anion exchange for light-emitting diodes. *ACS Appl Nano Mater*. 2020;3(2): 1766–1774.

[11] Zubko P, Gariglio S, Gabay M, et al. Interface physics in complex oxide heterostructures. *Annu Rev Condens Matter Phys*. 2011;2(1): 141–165.

[12] Fan J, Shavel A, Zamani R, et al. Control of the doping concentration, morphology and optoelectronic properties of vertically aligned chlorine-doped ZnO nanowires. *Acta Mater*. 2011;59(17): 6790–6800.

[13] Queisser HJ, Werner JH. *Principles and technology of photovoltaic energy conversion*. Paper presented at: 4th

International Conference on Solid-State and Integrated Circuit Technology; October 24–28, 1995; Beijing, China. https://ieeexplore.ieee.org/document/499656

[14] Fadla MA, Bentria B, Benghia A, et al. First-principles investigation on the stability and material properties of all-inorganic cesium lead iodide perovskites CsPbI3 polymorphs. *Phys B: Condens Matter*. 2020; 585: 412118.

[15] Busipalli DL, Lin KY, Nachimuthu S, Jiang JC. Enhanced moisture stability of cesium lead iodide perovskite solar cells–a first-principles molecular dynamics study. *Phys Chem Chem Phys*. 2020;22(10): 5693–5701.

[16] Alay-e-Abbas, SM, Nazir S, Noor NA, Amin N, Shaukat A. Thermodynamic stability and vacancy defect formation energies in SrHfO3. *J Phys Chem: C.* 2014;118(34): 19625–19634.

[17] Sutton R, Eperon G, Miranda L, et al. Bandgap-tunable cesium lead halide perovskites with high thermal stability for efficient solar cells. *Adv Energy Mater.* 2016;6(8): 1502458.

[18] Hong X, Ishihara T, Nurmikko AV. Dielectric confinement effect on excitons in PbI 4-based layered semiconductors. *Phys Rev: B.* 1992;45(12): 6961.

[19] Burgelman M, Nollet P, Degrave S. Modelling polycrystalline semiconductor solar cells. *Thin Solid Films.* 2000;361: 527–532.

[20] Andreev VM, Grilikhes VA, Rumiantsev VD. *Photovoltaic conversion of concentrated sunlight*. London: Wiley; 1997.

[21] Bloss WH, Pfisterer F, Schubert M, Walter T. Thin-film solar cells. *Prog Photovolt: Res Appl.* 1995;3(1): 3–24.

[22] Sievers RK, Hunt TK, Butkiewicz D, et al. *Prototype AMTEC cell development*. Paper presented at: International Energy Conversion Engineering Conference; August 07-12, 1994; Monterey, CA, US. https://arc.aiaa.org/doi/book/10.2514/MIECEC94

[23] Ita J, Stixrude L. Density and elasticity of model upper mantle compositions and their implications for whole mantle structure. In: E. Takahashi, R. Jeanloz and D. Rubie, eds. *Evolution of the Earth and Planets*. New York: American Geophysical Union; 1993: 111–130. doi:10.1029/GM074p0111

[24] Boinapally VR. *Computational study of structural and electrical properties of methylammonium lead iodide perovskite* [master's thesis]. Ohio: University of Toledo, College of Engineering; 2015.

[25] Lee MM, Teuscher J, Miyasaka T, Murakami TM, Snaith H. Efficient hybrid solar cells based on meso-superstructured organometal halide perovskites. *Science*. 2012;338(6107): 643–647.

[26] Lebedev AI. Ab initio calculations of phonon spectra in ATiO3 perovskite crystals (A= Ca, Sr, Ba, Ra, Cd, Zn, Mg, Ge, Sn, Pb). *Phys Solid State*. 2009;51(2): 362–372.

[27] Miura K, Azuma M, Funakubo H. Electronic and structural properties of ABO3: role of the BO coulomb repulsions for ferroelectricity. *Materials*. 2011;4(1): 260–273.

[28] Ashcroft NW, Mermin ND. *Solid state physics*. New York: Holt, Rinehart and Winston; 1976.

[29] Cahill DG, Pohl R. Lattice vibrations and heat transport in crystals and glasses. *Annu Rev Phys Chem.* 1988;39(1): 93–121.

[30] Levy GC, Hunt TK, Sievers RK. *AMTEC: current status and vision*. Paper presented at: 32nd Intersociety Energy Conversion Engineering Conference, IECEC-97. IEEE; 1997. https://ieeexplore.ieee.org/abstract/document/661931

[31] Cole T. Thermoelectric energy conversion with solid electrolytes. *Science*. 1983;221(4614): 915–920.

[32] Tsymbal EY, Kohlstedt H. *Tunneling across a ferroelectric*. *Science*. 2006;313(5784): 181–183. doi: 10.1126/science.1126230

[33] Huang, Y-H, Dass RI, Xing Z-L, Goodenough JB. Double perovskites as anode materials for solid-oxide fuel cells. *Science*. 2006;312(5771): 254–257. doi: 10.1126/science.1125877

[34] Yamada H, Ogawa Y, Ishii Y, et al. Engineered interface of magnetic oxides. *Science*. 2004;305(5684): 646–648. doi: 10.1126/science.1098867

[35] Shannon RD. Revised effective ionic radii and systematic studies of interatomic distances in halides and chalcogenides. *Acta Cryst Section A*. 1976;32(5): 751–767.

[36] Makino K, Tomita K, Suwa K. Effect of chlorine on the crystal structure of a chlorine-rich hastingsite. *Mineral Mag*. 1993;57(389): 677–686.

[37] Li T-I, Stucky GD, McPherson G. The crystal structure of $CsMnCI_3$ and a summary of the structures of RMX_3 compounds. *Acta Cryst Section B*. 1973;29: 1330. http://scripts.iucr.org/cgi-bin/paper?S0567740873004450

[38] Groat LA, John LJ, Bonnie CP. The crystal structure of argentojarosite, AgFe3 (SO4) 2 (OH) 6. *Can Mineral*. 2003;41(4): 921–928.

[39] Howie RA, Moser W, Trevena IC. The crystal structure of tin (II) iodide. *Acta Cryst Section B*. 1972;28(10): 2965–2971.

[40] Tomioka Y, Okimoto Y, Jung JH, Kumai R, Tokura Y. Phase diagrams of perovskite-type manganese oxides. *J Phys Chem Solids*. 2006;679(9): 2214–2221. https://ui.adsabs.harvard.edu/abs/2006JPCS...67.2214T/abstract

[41] Reaney IM, Iddles D. Microwave dielectric ceramics for resonators and filters in mobile phone networks. *J Am Ceram Soc*. 2006;89(7): 2063–2072.

[42] Hirata T, Ishioka K, Kitajima M. Vibrational spectroscopy and X-ray diffraction of perovskite compounds Sr 1− x M x TiO 3 (M= Ca, Mg; 0≤ x≤ 1). *J Solid State Chem*. 1996;124(2): 353–359.

[43] Kazim S, Nazeeruddin, Gratzel M, Ahmad S. Perovskite as light harvester: a game changer in photovoltaics. *Angew Chem*. 2014;53(11): 2812–2824.

[44] Alger DL. *Some corrosion failure mechanisms of AMTEC cells*. Paper presented at: 32nd Intersociety Energy Conversion Engineering Conference, IECEC-97. IEEE; 1997. https://ieeexplore.ieee.org/abstract/document/661943

[45] Bankston CP, Shirbacheh M. *AMTEC: high efficiency static conversion for space power* (Working group papers, V. 2, Sect. 5). Marshall Space Flight Center Manned Mars Mission; 1986: 715–732. https://ui.adsabs.harvard.edu/abs/1986mmm..work..715B/abstract

[46] Ryan M, Kisor A, Williams R, Jeffries B-N, O'Connor D. *Lifetimes of thin film AMTEC electrodes*. Paper presented at: International Energy Conversion Engineering Conference; August 07-12, 1994; Monterey, CA, US. https://doi.org/10.2514/6.1994-3831

[47] Perdew JP, CHevary JA, Vosko SH, et al. Atoms, molecules, solids, and surfaces: applications of the generalized gradient approximation for exchange and correlation. *Phys Rev B.* 1992;46(11): 6671. https://journals.aps.org/prb/abstract/10.1103/PhysRevB.46.6671

[48] Kohn W, Sham LJ. Self-consistent equations including exchange and correlation effects. *Phys Rev.* 1965;140(4A): A1133.

[49] Payne MC, Teter MP, Allan DC, Arias TA, Joannopoulos JD. Iterative minimization techniques for ab initio total-energy calculations: molecular dynamics and conjugate gradients. *Rev Mod Phys.* 1992;64(4): 1045.